Polymer 49 (2008) 2553–2559

Contents lists available at ScienceDirect

Polymer

journal homepage: www.elsevier.com/locate/polymer

Composition fluctuations before dewetting in polystyrene/poly(vinyl methyl ether) blend thin films

Hiroki Ogawa, Toshiji Kanaya*, Koji Nshida, Go Matsuba

Institute for Chemical Research, Kyoto University, Uji, Kyoto-fu 611-0011, Japan

ARTICLE INFO

Article history:
Received 21 November 2007
Received in revised form 11 February 2008
Accepted 15 March 2008
Available online 28 March 2008

Keywords:
Polymer blend thin film
Phase separation
Dewetting

ABSTRACT

We report structural development in blend thin films of deuterated polystyrene (dPS) and poly(vinyl methyl ether) (PVME) below ~200 nm in two phase region during the incubation period before dewetting using neutron reflectivity (NR) and atomic force microscopy (AFM). As was predicted by the former optical microscope (OM) and small-angle light scattering (LS) measurements on blend thin films of protonated PS and PVME [Ogawa H, Kanaya T, Nishida K, Matsuba G. Polymer 2008;40:254–62.], the NR results clearly showed that the tri-layer structure consisting of the surface PVME layer, the middle blend layer and the bottom PVME layer was formed in the one phase region. After the temperature jump into the two phase region, it was found that the phase separation of the middle blend layer proceeded in the depth direction during the incubation period before dewetting, suggesting that the dewetting was induced by the composition fluctuations during the incubation period.

1. Introduction

Extensive studies have been performed on polymer thin films including single component and multi-component systems [1–4] because properties of polymer thin films are directly related to many important phenomena such as coating, adhesion, surface friction, lubrication, and surface dielectric constant. The studies on polystyrene (PS) thin films on Si substrates have revealed that glass transition temperature T_g decreased with film thickness d below about 40 nm [5–9], but increased with decreasing film thickness d for poly(methyl methacrylate) (PMMA) [5,6], showing the importance of interactions between polymers and substrates. Recently, dewetting and phase separation of polymer blend thin films are also of great interest because of technological applications as well as fundamental investigations. The dewetting of the phase separated polymer blend thin film limits the industrial applications because they require stable, homogeneous and uniform thin films. This motivated the fundamental studies on polymer blend thin films very much to reveal the dewetting mechanism and control the morphology [4] for blend thin films of poly(*p*-methylstyrene) (P*p*MS) and deuterated polystyrene (dPS) [10], poly(styrene-*ran*-acrylonitrile) (SAN) and deuterated poly(methyl methacrylate) (dPMMA) [11–15], and PS and poly(vinyl methyl ether) (PVME) [16–19] in various film thickness ranges.

As for the dewetting Composto and Wang [13,14] have proposed the capillary fluctuation mechanism for the blend thin films of SAN and dPMMA ($R_g < d < 150R_g$, R_g being radius of gyration of a polymer). On the other hand, Chung et al. [20] have recently shown that the phase separation in thin films of SAN and dPMMA ($d = 550$ nm) drove the dewetting and the capillary fluctuations failed to explain the dewetting. Liao et al. [15] have experimentally demonstrated that the composition fluctuation mechanism [21–24] induced the dewetting in thermodynamically stable ultrathin blend films of SAN and dPMMA in one phase region. Thus, the dewetting mechanism in blend thin films is still a controversial problem.

In a previous paper [25], therefore, we investigated morphology and kinetics of phase separation as well as dewetting in blend thin films of PS/PVME on glass substrate in two phase region as a function of film thickness in a wide thickness d range from 65 μm to 42 nm ($\sim 2.5R_g$) to elucidate the relation between phase separation and dewetting. We found that the dewetting occurred in a spinodal decomposition (SD) mechanism after a long incubation time in a thickness range below ~200 nm. The observations indicated that a layered structure was formed in the incubation time before the dewetting although direct evidences for the layered structure were not obtained in the previous work. In order to confirm the prediction of the layered structure we have mainly studied structural development in the depth direction during the incubation period before the dewetting for thin blend films of deuterated PS (dPS) and PVME in a thickness range below ~200 nm using neutron reflectivity.

2. Experiment

Polystyrene (PS) and poly(vinyl methyl ether) (PVME) used in this study have weight-average molecular weights $M_w = 280{,}000$

* Corresponding author. Tel.: +81 774 38 3140; fax: +81 774 38 3146.
E-mail address: kanaya@scl.kyoto-u.ac.jp (T. Kanaya).

0032-3861/$ – see front matter © 2008 Elsevier Ltd. All rights reserved.
doi:10.1016/j.polymer.2008.03.034

and 90,000, and the molecular weight distributions in terms of $M_w/M_n = 3.01$ and 1.88, respectively, where M_n is number-average molecular weight. We also used deuterated polystyrene (dPS) with weight-average molecular weight $M_w = 280{,}000$ and the molecular weight distribution $M_w/M_n = 1.08$ for neutron reflectivity measurements. Both PS (dPS) and PVME were purchased from Scientific Polymer Products, Inc. PS (dPS) and PVME were purified by precipitating the toluene solutions into excess methanol and *n*-heptane several times, respectively, and dried in vacuum at room temperature for 72 h. Films below and above 1 μm were prepared by spin-coating and casting the toluene solution of PS and PVME, respectively, on a cleaned glass substrate after filtering with 2 μm pore size membrane at room temperature for optical microscopy (OM), atomic force microscopy (AFM) and small-angle light scattering (LS). The films were then annealed at 60 °C for 24 h after drying in vacuum at room temperature for 24 h. Thickness of polymer film was controlled by varying the polymer concentration in solution and confirmed with ellipsometric measurements. Blend films of dPS and PVME were prepared on a cleaned Si wafer with native oxide layer in the same manner as for the PS and PVME films.

The phase diagram of PS and PVME has been determined in the previous work [25], which is a lower critical solution temperature (LCST) type phase diagram. The critical weight fraction of PS is 0.3 and the critical temperature is 104.5 °C. All the measurements were done on the blend samples with the critical concentration. The glass transition temperature T_g of the bulk blend with the critical concentration $\phi_{PS} = 0.3$ is −20 °C. The coexisting compositions are nearly pure components at 115 °C, which were estimated by extrapolating the phase diagram.

Small-angle light scattering (LS) measurements were carried out using home-made apparatus with confocal collimation, which enables us to access a very low q range down to 0.1 μm^{-1} with extremely low background. Two-dimensional scattering intensities were accumulated every 5 min after temperature jump from one phase region to two phase region (= 115 °C) with a heating rate of 36 °C/min. Details of the LS instrument were reported elsewhere [26]. Optical microscopic (OM) and confocal laser scanning microscopic (CLSM) measurements were also done after temperature jump from one phase region to two phase region (= 115 °C) using OLYMPUS BX50 equipped with a CCD camera and LASER TECH. ILM15, respectively. Atomic force microscopic (AFM) measurements were performed at room temperature after quenching the sample from two phase region (= 115 °C) using JEOL JSPM-4200 to examine the surface morphology of the films.

Neutron reflectivity measurements were done on MINE-II reflectometer at JRR-3 reactor in Tokai [27]. Incident neutron wavelength was 0.88 nm and the q range covered in the present measurements was 0.07–1.0 nm^{-1}. The measurements were conducted at room temperature after quenching the sample from two phase region (= 115 °C). We analyzed the observed reflectivity data using the Paratt32 program in Hahn–Meitner Institute [28], which is based on a recursion formula derived by Parratt [29] to calculate reflectivity from successive interfaces and modified to include effects of interfacial roughness.

3. Results and discussion

We first recall the previous results [25] to clarify the aim of this work. We have studied the phase separation and dewetting processes of blend thin films of PS and PVME with the critical concentration in a wide thickness range of 42 nm to 65 μm after a temperature jump to 115 °C in the two phase region from the one phase region using OM, AFM and LS. We found that both the phase separation and dewetting processes depended on the film thickness, and were classified into four thickness regions. In order to explain the characteristic features in the four regions the typical OM and AFM images at 90 min after the temperature jump are shown in Fig. 1(a) and (b), respectively, and the time evolutions of the LS profiles are shown in (c) for the four regions. In the first region above ∼15 μm (Region I), the spinodal decomposition (SD) type phase separation is observed in the OM image, which is also confirmed from the time evolution of LS intensity. In this region no dewetting is observed in the AFM image, and hence this region can be regarded as bulk region. In the second region between ∼15 μm and ∼1 μm (Region II) the SD type phase separation proceeds in the early stage similar to Region I while the characteristic wavelength decreases with the film thickness due to the confinement effect of film thickness in this region. In the late stage the dewetting is induced by the phase separation. In the third region between ∼1 μm and ∼200 nm (Region III) the dewetting is observed *even* in the early stage. The dewetting morphology is very irregular as seen in Fig. 1(a) and (b) and no definite characteristic wavelength is observed in the LS profile. It is expected that the irregular morphology is induced by mixing up the characteristic wavelengths of the phase separation and the dewetting. In the forth region below ∼200 nm (Region IV) the dewetting occurs after a long incubation time with a characteristic wavelength, giving a peak in the LS profile as seen in Fig. 1(c). Note that the LS profiles in Fig. 1(c) are shown until 60 min for Region IV. Generally speaking, the SD type mechanism occurs in an unstable region [30,31], meaning that no incubation time is required. However, the long incubation time is observed before the dewetting, suggesting that some structural formation occurs before the onset of the SD type dewetting. Therefore, we examined structural formation in the incubation period before dewetting to discuss the dewetting mechanism in Region IV below ∼200 nm.

In Fig. 2, time evolution of the OM images is shown for the 98 nm film after temperature jump to 115 °C to see what happens in the incubation period. Nothing is observed in the OM images before ∼20 min within the present OM contrast and the spatial resolution while very weak in-plane fluctuations are recognized after ∼20 min as seen in Fig. 2. At ∼30 min the SD type patterns become rather clear and grow in size with the annealing time. According to the changes in the OM images, we also observe the changes in the LS profiles. In Fig. 3 we plot the time evolution of the LS intensity I_{max} and the peak position q_{max}. The LS peak appears at 30 min after the temperature jump, corresponding to the appearance of the SD pattern in the OM image. It is noted that the LS intensity slightly increases until ∼30 min in the incubation period, which must be due to the very weak in-plane fluctuations observed in the OM image. After ∼30 min the peak intensity I_{max} increases rapidly with the annealing time and the peak position shifts to lower q. It is clear from the AFM images in Fig. 1(b) that this SD type pattern is caused by the dewetting.

As discussed in the previous paper [25] we expect that some layered structure is formed during the incubation period, and triggers the dewetting through the capillary fluctuations mechanism [13,14] or the composition fluctuation one [15,21–24]. However, no direct evidence was provided for the layered structure. In order to confirm the layered structure we examined the composition fluctuations in the direction normal to the surface (the depth direction) before dewetting using neutron reflectivity (NR), which is one of the most powerful tools to study composition and/or density fluctuations in the depth direction.

We used a Si wafer as a substrate in the NR measurements instead of a glass substrate, which was used for OM, LS and AFM in the previous paper [25]. It is known that the dewetting is affected by interface interactions between polymer film and substrate. In addition we used deuterated polystyrene (dPS) in the NR experiments. It would be impossible to consider these two systems (PS/PVME on a glass substrate and dPS/PVME on a Si substrate) are identical. Therefore we first examined the dPS/PVME blend film of

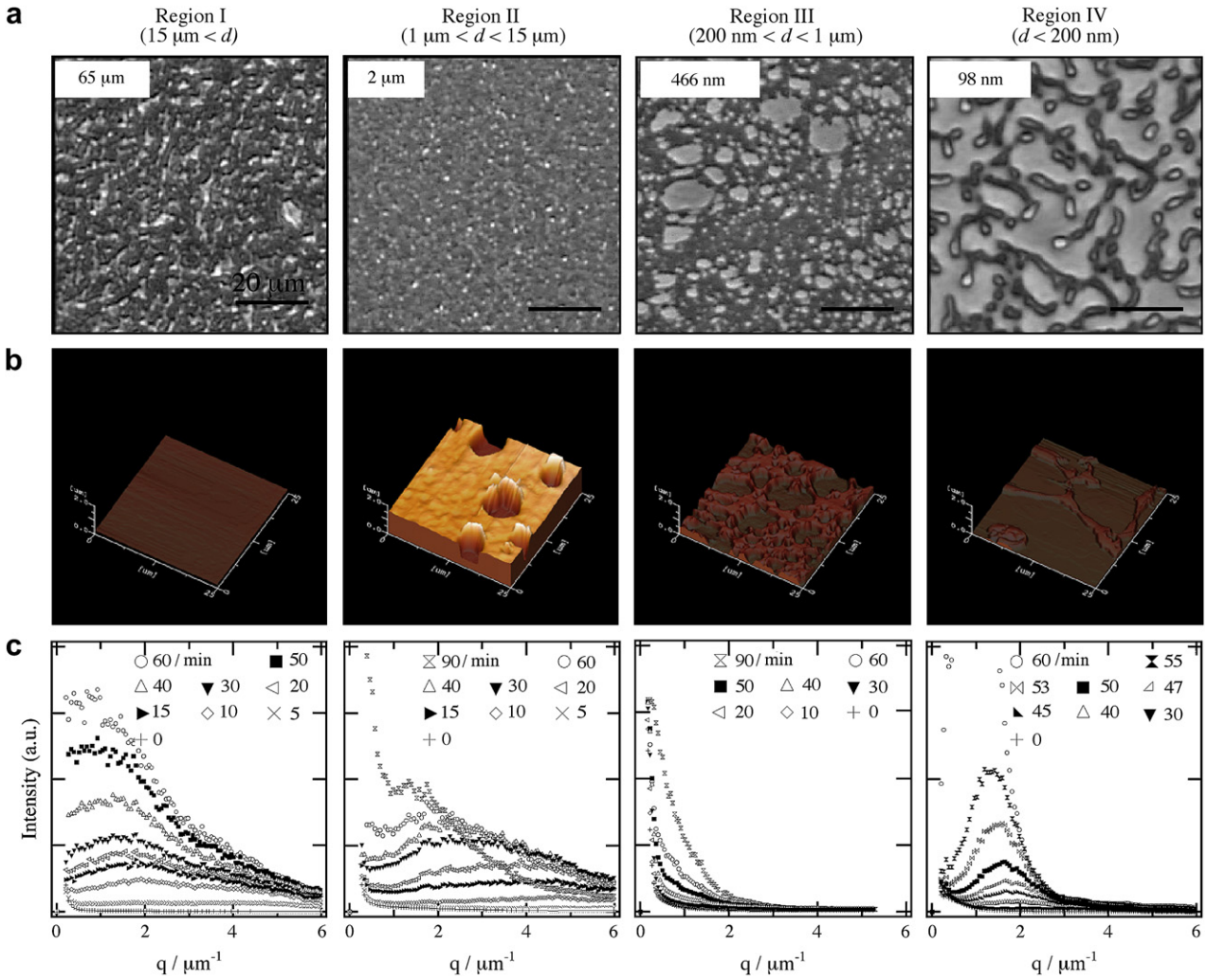

Fig. 1. OM (a) and AFM (b) images of PS/PVME blend thin films after temperature jump to 115 °C in the two phase region for four thickness d regions. Region I (15 μm < d): 65 μm, Region II (1 μm < d < 15 μm): 2 μm, Region III (200 nm < d < 1 μm): 466 nm, Region IV (d < 200 nm): 98 nm and time evolution of LS profiles (c) after temperature jump to 115 °C in the two phase region. Scale bars in OM images are 20 μm. Z-range is 2.0 μm and x–y size is 25 μm × 25 μm for all AFM images.

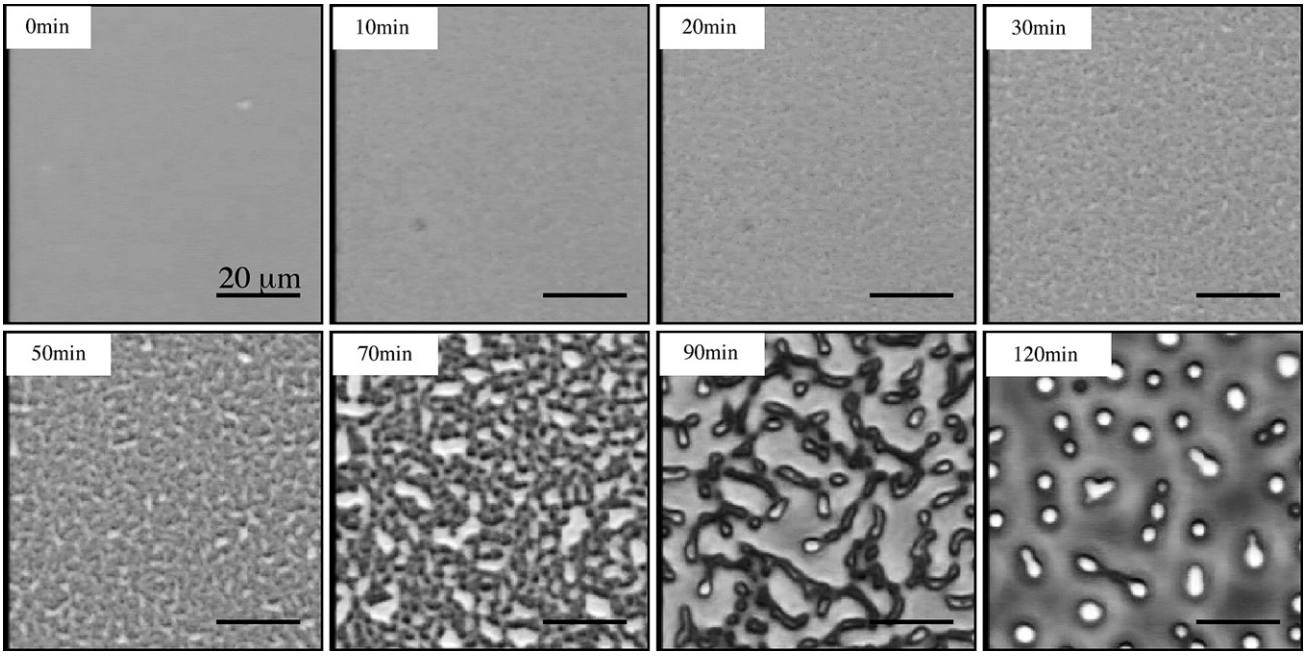

Fig. 2. Time evolution of OM images of PS/PVME blend film of 98 nm thickness after temperature jump to 115 °C in the two phase region. Scale bars in OM images are 20 μm.

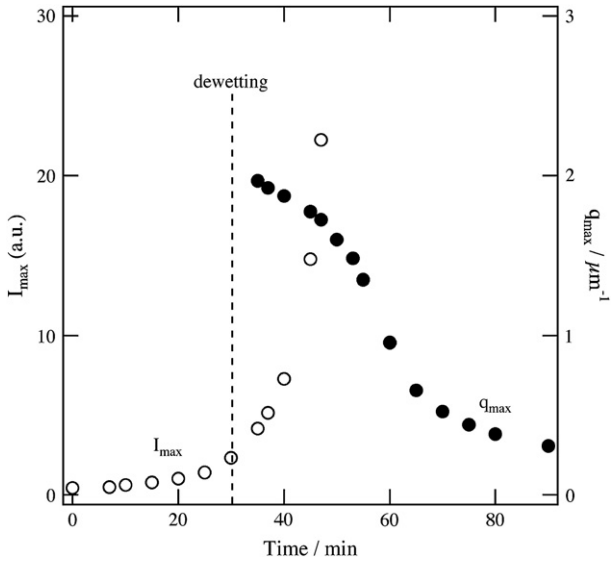

Fig. 3. Time evolution of peak position q_{max} and peak intensity I_{max} in the LS profile of PS/PVME blend film of 98 nm thickness after temperature jump to 115 °C in the two phase region. Peak intensity I_{max} in the incubation period before ~30 min is intensity at $q = 2\ \mu m^{-1}$.

98 nm thickness using confocal laser scanning microscope (CLSM). We found that the dewetting patterns were almost identical but the onset time was slower in the case of the Si substrate than the glass one. Exactly speaking, it is 60 min at 115 °C for the Si substrate and 30 min for the glass substrate. No other large differences were observed between the Si and the glass substrates. However, the phase separation and dewetting are strongly affected by the substrates so that we discuss the results on the dPS/PVME thin films on the Si substrate independent of the PS/PVME thin films on the glass substrate in this paper.

We performed NR measurements on the dPS/PVME blend films at room temperature in the one phase region before annealing at 115 °C in the two phase region. The observed NR profiles are shown in Fig. 4 for the 180 nm, 98 nm, 42 nm and 25 nm films. The well defined fringed patterns were observed in the profiles. The NR profiles were analyzed by fitting a single layer model on a Si substrate with a native oxide layer to the observed data, but good fitness was not obtained. Then, we tried bi-layer and tri-layer models consisting of surface PVME layer at the air, middle blend layer, and interface PVME layer at the Si substrate because the preferential interactions are considered between PVME and air [32–36] and between PVME and Si substrate [17,18]. In this model the surface roughness $\sigma_{NR,surf}$ and the interface roughness $\sigma_{NR,inter}$ were introduced by an error function (Eq. (1))

$$\mathrm{erf}(x) = \int_x^\infty \frac{1}{\sqrt{2\pi}\sigma_i}\exp\left(-\frac{t^2}{2\sigma_i^2}\right)\mathrm{d}t \quad (i = \mathrm{NR,inter\ or\ NR,surf}) \tag{1}$$

It was found that the tri-layer model gave good agreements between the observed reflectivity and the calculated one as shown in Fig. 4. In the inset of Fig. 4 the scattering length density evaluated in the fit is shown for each film. The estimated surface and interface PVME layers are ~4 nm and ~5 nm thick and almost independent of the total film thickness within the experimental error. The surface roughness, the interface roughness between the surface PVME layer and the middle blend layer and the interface roughness between the middle blend layer and the bottom PVME layer are 3.5 nm, 4.5 nm and 5 nm for the 180 nm film, respectively, and slightly decrease with the total film thickness. It is expected that the surface and interface PVME layer formation increase the dPS concentrations in the middle blend layer, especially in the thin

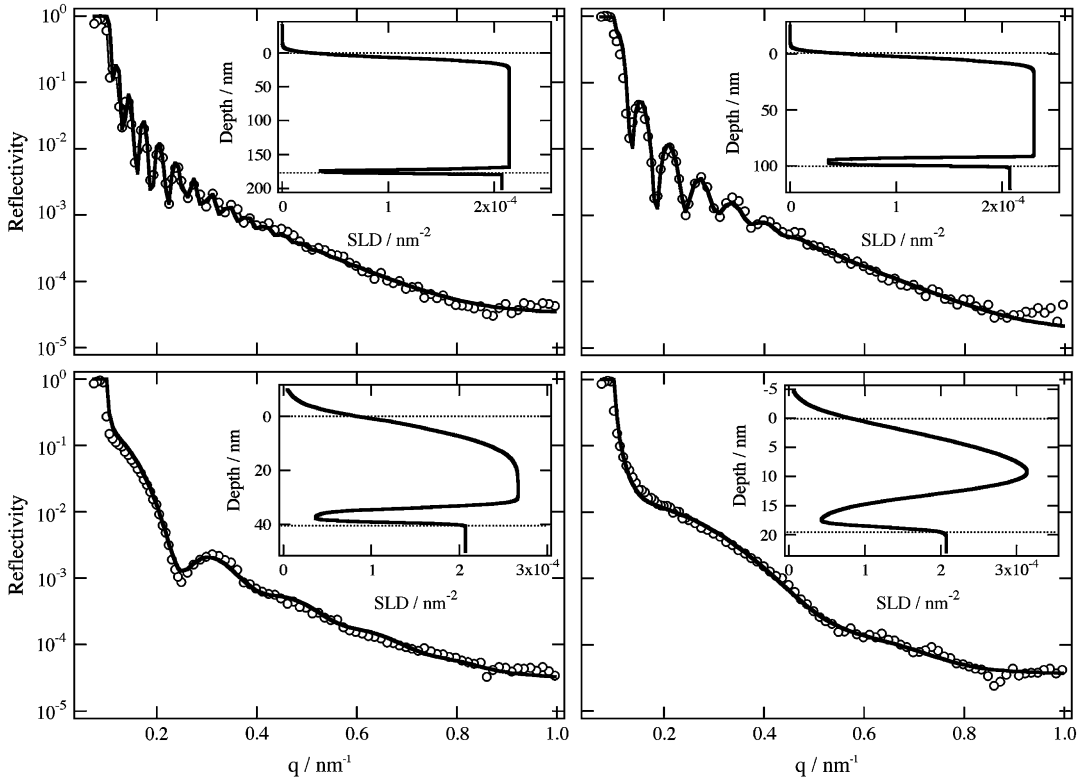

Fig. 4. NR profiles for dPS/PVME blend films of 180 nm, 98 nm, 42 nm and 25 nm thickness at 25 °C in the one phase region and the results of fits (solid curves) with the tri-layer model. Insets show scattering length density (SLD) profiles in depth direction evaluated in the NR profile fits.

films. Hence, we have evaluated the PS concentrations in the middle blend layer and found that the effect is negligible for the 180 nm and 98 nm films, but not negligible for the 42 nm and 25 nm films. In the case of the 25 nm film the estimated dPS concentration ϕ_{PS} in the middle blend layer is 0.47. Therefore, further experiments were performed on the 98 nm film. In any case the present results clearly show that the dPS/PVME blend thin films on the Si substrate have tri-layer structure even in the one phase region due to the preferential interactions.

In the next step we have examined the time evolution of the tri-layer structure in the 98 nm film during the incubation period before the dewetting. The film was annealed at 115 °C in the two phase region for a given period, and quenched to room temperature in the one phase region. The NR measurements were performed on the quenched film. In Fig. 5(a) the observed NR profiles are shown for various annealing periods. The fringed pattern is gradually smeared with the annealing time even in the incubation period (~60 min), suggesting that the surface roughness and/or the interface roughness increases with the annealing time before the dewetting. At 120 min the fringed pattern is completely smeared out, showing the film is dewetted. It is surprising that the fringed pattern with a long period was again observed at 360 min, implying that a thin layer was formed on the surface of the substrate after the dewetting. This problem will be discussed later.

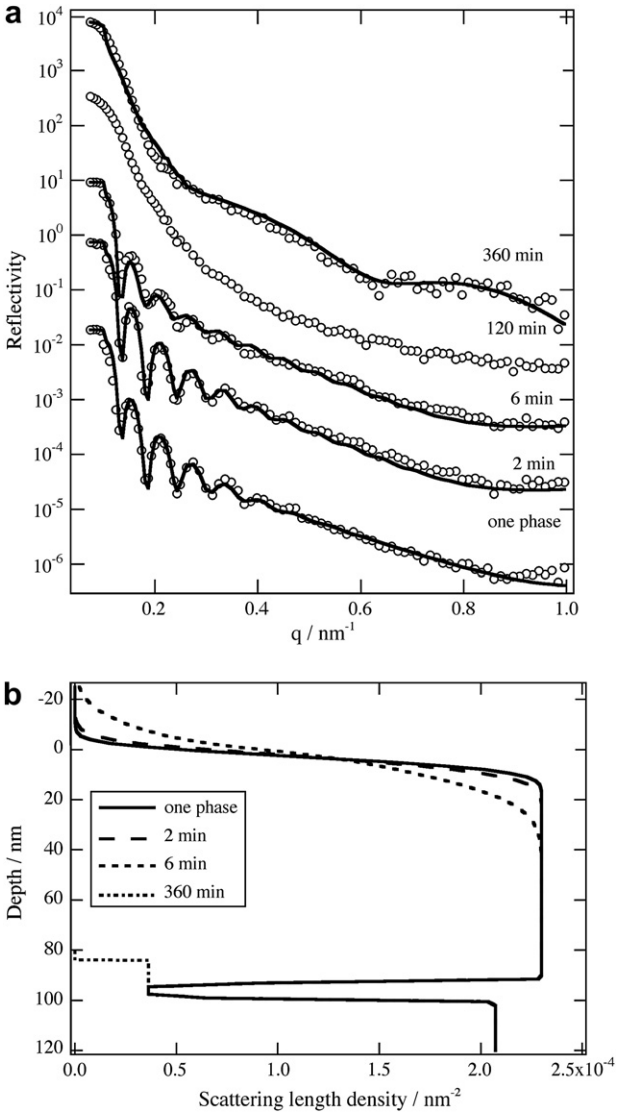

Fig. 5. (a) Time evolution of NR profile for dPS/PVME blend film of 98 nm thickness annealed at 115 °C in the two phase region. Measurements were done after quenching to room temperature. The solid curves are the results of fits with the tri-layer model. (b) Scattering length density (SLD) profiles in depth direction as a function of annealing time.

The NR profile calculated from the tri-layered model was fitted to the observed one to evaluate the thickness and the surface roughness and interfacial roughness for each layer. The results of fits are shown by solid curves in Fig. 5(a) and the depth profiles of the corresponding scattering length density are plotted in (b). The interface roughness $\sigma_{NR,inter}$ between the top PVME layer and the middle blend layer increases with the annealing time during the induction period, but the interface roughness between the bottom PVME layer and the middle blend layer stays almost constant (~5 nm). The surface roughness $\sigma_{NR,surf}$ of the top PVME layer seems to increase with the annealing time, but it is noted that the NR profile is not sensitive to the surface roughness of the top PVME layer because of the low scattering length density of PVME so that we do not discuss the surface roughness here. The former interface roughness $\sigma_{NR,inter}$ is plotted as a function of the annealing time in Fig. 6. It is evident that they increase even during the incubation period. Before going to the discussion on the time evolution of the roughness, we introduce the surface roughness $\sigma_{AFM,surf}$ evaluated by the AFM measurements because the surface roughness $\sigma_{NR,surf}$ estimated by the NR measurements includes large error.

The observed AFM images of the dPS/PVME film of 98 nm thickness are shown in Fig. 7 for various annealing times in the incubation period. The surface is very smooth at the annealing time = 0 min. As the annealing proceeds no significant changes were observed during the incubation period. In order to evaluate the surface roughness the AFM data were analyzed in the following way. The distribution of surface heights h was calculated from the AFM data. An example is shown in Fig. 8 for the 98 nm film annealed at 115 °C for 5 min. Assuming a Gaussian distribution of h, the standard deviation $\sigma_{AFM,surf}$ was evaluated by fitting Eq. (2) to the observed distribution.

$$f(h) = \frac{1}{\sqrt{2\pi}\sigma_{AFM,surf}} \exp\left(-\frac{(h-\bar{h})^2}{2\sigma^2_{AFM,surf}} \right) \quad (2)$$

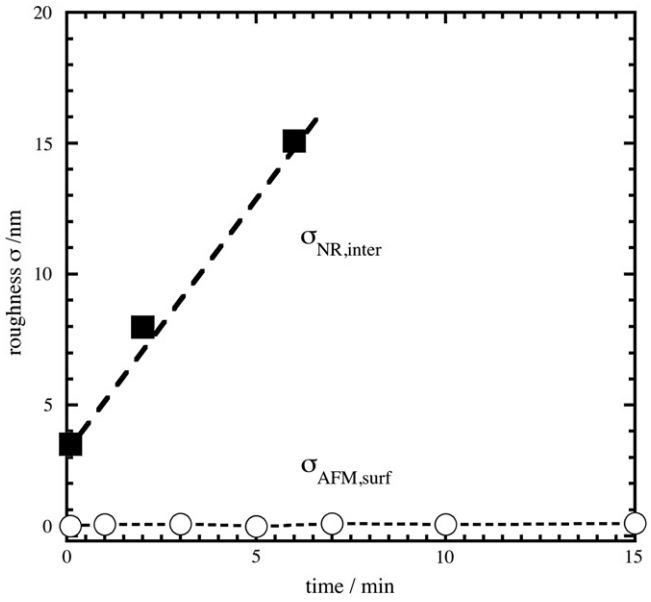

Fig. 6. Time evolutions of interface roughness $\sigma_{NR,inter}$ evaluated from the NR data and the surface roughness $\sigma_{AFM,surf}$ from AFM data, respectively, for dPS/PVME blend film of 98 nm thickness annealed at 115 °C in the two phase region.

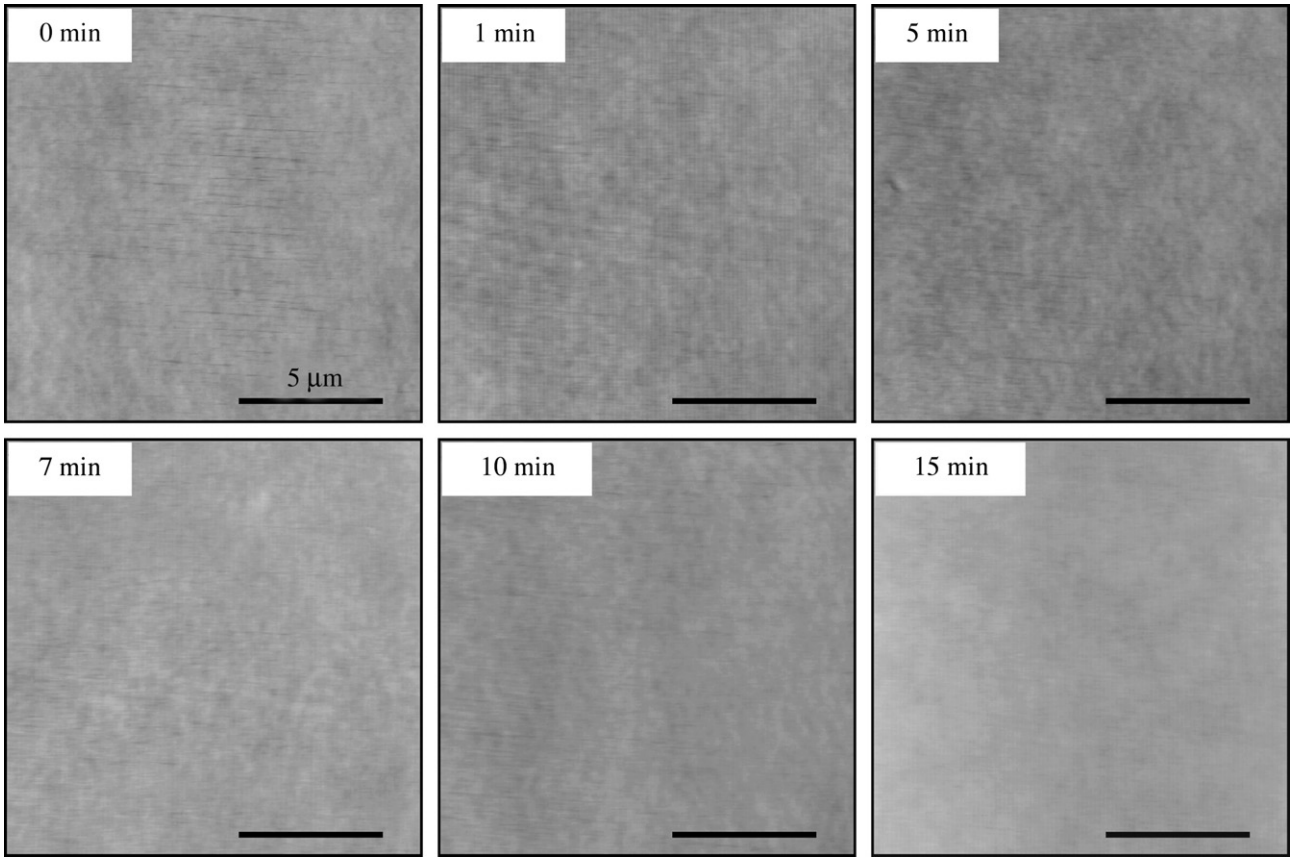

Fig. 7. Time evolution of AFM images of dPS/PVME blend film of 98 nm thickness after temperature jump to 115 °C in the two phase region. Scale bars in AFM images are 5 μm.

where $\bar{h}$ is the average value of the height. The result of fit is shown by a solid curve in the figure. As seen in Fig. 8 the distribution is well described by a Gaussian function in the incubation period. The evaluated surface roughness $\sigma_{AFM,surf}$ is plotted in Fig. 6 as a function of the annealing time in the incubation period to compare with the interface roughness $\sigma_{NR,inter}$ evaluated by the NR measurements.

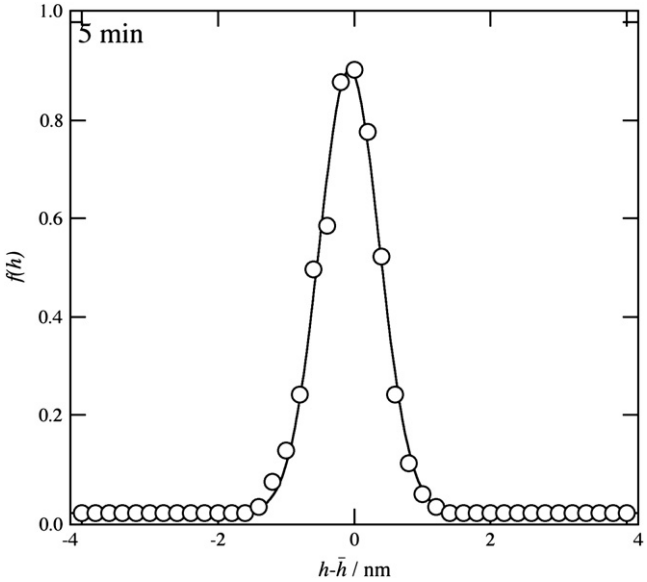

Fig. 8. Distribution $f(h)$ of surface heights in the surface of dPS/PVME film of 98 nm thickness annealed at 115 °C for 5 min. The solid curve is result of fit to a Gaussian function.

The AFM surface roughness $\sigma_{AFM,surf}$ is almost independent of the annealing time. On the other hand, the interface roughness $\sigma_{NR,inter}$ increases with the annealing time from the beginning of the incubation time. In the two phase region it is expected that the phase separation would occur in the middle blend layer into PVME-rich and dPS-rich phases. Nevertheless, no changes were observed during incubation period in the CLMS images, suggesting that the phase separation dose not proceed at least in the in-plane direction. The increase of the NR interface roughness $\sigma_{NR,inter}$ in the incubation period indicates that the phase separation proceeds in the depth direction, which must be induced and accelerated by the preferential interactions between PVME and air [35]. This phase separation in the depth direction does not occur coherently in the depth direction like the surface directed spinodal decomposition (SDSD) [37], but inhomogeneously in the in-plane direction [15].

In the following we will discuss the dewetting mechanism on the basis of the observations. In the previous paper [25] we considered two possibilities for the dewetting mechanism for the PS/PVME thin films in Region IV below ~200 nm: the capillary fluctuation mechanism [13,14] and the composition fluctuation mechanism [15,21–24]. The former mechanism was proposed by Composto and Wang [13,14] to explain the dewetting of deuterated poly(methyl methacrylate) (dPMMA) and poly(styrene-*ran*-acrylonitrile) (SAN) in a thickness d range of $R_g < d < 150R_g$. In order to check the mechanism we evaluated the capillary fluctuation for the interface between the surface PVME and the middle blend layer based on the theory by Shull et al. [38]. It was found that the fluctuation length was less than 3.3 nm, which is much smaller than the interface roughness derived from the NR result in the incubation period, implying a less possibility of the capillary fluctuation mechanism.

The composition fluctuation mechanism was theoretically introduced by some researchers [21–24] and An and coworkers [15] applied this idea to explain the dewetting of thermodynamically stable blend ultrathin film of dPMMA and SAN with $d \sim R_g$. In this mechanism polymers which have preferable interactions with the surface (or the substrate) diffuse to the surface (or the substrate) so as to create the composition gradient across the film. The diffusion could not occur homogeneously over the film surface to create the composition fluctuations in the mixture along the surface. When the amplitude of the fluctuations is large enough, the free surface is eventually destabilized, leading to the dewetting [21–24]. This mechanism is also possible in the two phase region. In the present experiment we observed tri-layer structure in the dPS/PVME blend thin film of 98 nm thickness. The film was stable in the one phase region and no dewetting occurs. After the temperature jump into the two phase region, however, we found that the interface roughness $\sigma_{NR,inter}$ increases rapidly with the annealing time in the incubation period, showing that the composition fluctuations proceed in the depth direction with the annealing time, and the composition fluctuations may proceed inhomogeneously in the in-plane direction. These inhomogeneous composition fluctuations must induce the dewetting when the amplitude is large enough that the surface is destabilized. Thus, the present observations support the composition fluctuation induced dewetting mechanism for the dPS/PVME blend film below ~200 nm.

Finally we would like to comment on the fringed pattern observed in the NR profile at 360 min after the temperature jump in Fig. 5(a). The fringed pattern with a long period suggests that a very thin PVME layer is formed in a very late stage after the dewetting. The thickness evaluated by fitting is ~10 nm, which is shown in the scattering length density profile in Fig. 5(b). Why does such a thin film is formed after the dewetting? In the incubation period the phase separation occurs mainly in the depth direction, but when the dewetting occurs at around 60 min after the temperature jump the phase separation is not completed. After the dewetting into the droplets the phase separation may proceed within the droplets. Outer surface of the droplets must be PVME because of the preferential interactions between PVME and air [32–36]. The phase separation further proceeds and the surface PVME increases in thickness. Finally PVME comes out from the surface of the droplets onto the substrate to form a very thin layer of 10 nm thickness. Similar thin film formation was reported by Stamm et al. [10] after a very long annealing of dPS and P*p*MS blend thin films.

4. Conclusion

In this study we investigated structural development of blend thin films of dPS (PS) and PVME below ~200 nm at 115 °C in the two phase region during the incubation period before the dewetting. It was found in the NR measurements that the thin film had a tri-layer structure consisting of the surface PVME layer, the middle blend layer and the bottom PVME layer even in the one phase region. This must be due to preferable interactions of PVME and air and PVME and Si substrate. When the thin film was annealed at 115 °C the interfacial roughness $\sigma_{NR,inter}$ between the top PVME and the middle blend layer rapidly increased with the annealing time. This is the phase separation of the middle layer enhanced by the preferable interaction between PVME and air. This observation supported the dewetting mechanism induced by composition fluctuations. After very long annealing of 360 min the NR result clearly showed that a thin PVME layer was formed on the Si substrate. It implies that the phase separation proceeds in the dewetted droplets, and the inner PVME comes out, and finally wets the Si surface.

References

[1] Jones RL, Richards RW. Polymers at surface and interfaces. Cambridge: Cambridge University Press; 1999.
[2] Karim A, Kumar S. Polymer surfaces, interfaces and thin films. Singapore: World Scientific; 2000.
[3] Bucknall DG. Prog Mater Sci 2004;49:713–86.
[4] Mueller-Buschbaum P, Bauer E, Wunnicke O, Stamm M. J Phys Condens Matter 2005;17:S363–86.
[5] Keddie JL, Jones RA, Cory RA. Europhys Lett 1994;27:59–64.
[6] Keddie JL, Jones RA, Cory RA. Faraday Discuss 1994;98:219–30.
[7] Forrest JA, Dalnoki-Veress K, Stevens JR, Dutcher JR. Phys Rev Lett 1996;77:2002–5.
[8] Kawana S, Jones RAL. Phys Rev E 2001;63:021501.
[9] Miyazaki T, Nishida K, Kanaya T. Phys Rev E 2004;69:06183–8.
[10] Mueller-Buschbaum P, O'Neil SA, Affrossman S, Stamm M. Macromolecules 1998;31:5003–9.
[11] Chung H, Composto RJ. Phys Rev Lett 2004;92:185704.
[12] Wang H, Composto RJ. Europhys Lett 2000;50:622–7.
[13] Wang H, Composto RJ. Chem Phys 2000;113:10386–97.
[14] Wang H, Composto RJ. Interface Sci 2003;11:237–48.
[15] Liao Y, Su Z, Sun Z, Shi T, An L. Macromol Rapid Commun 2006;27:351–5.
[16] Tanaka K, Yoon JS, Takahara A, Kajiyama T. Macromolecules 1995;28:934–8.
[17] Ermi BD, Karim A, Douglas JF. J Polym Sci Part B 1998;36:191–200.
[18] Karim A, Slawecki TM, Kumar SK, Douglas JF, Satija SK, Han CC, et al. Macromolecules 1998:857–62.
[19] El-Mabrouk K, Belaiche M, Bousmina M. J Colloid Interface Sci 2007;306:354–67.
[20] Chung HJ, Ohno K, Fukuda T, Composto TJ. Macromolecules 2007;40:384–8.
[21] Wensink KDF, Jéremoe B. Langmuir 2002;18:413–6.
[22] Sharma A, Mittal J. Phys Rev Lett 2002;89:1861.
[23] Sharma A, Mittal J, Verma R. Langmuir 2002;18:10213–20.
[24] Clarke N. Macromolecules 2005;38:6775–8.
[25] Ogawa H, Kanaya T, Nishida K, Matsuba G. Polymer 2008;40:254–62.
[26] Nishida K, Kanaya T, Matsuba G, Ogawa H, Konishi T. Japanese Patent Pending 2005-058211; 2005.
[27] Ebisawa T, Tasaki S, Otake Y, Funahashi H, Soyama K, Torikai N, et al. Physica 1995;B213/214:901–3.
[28] Braun C. Parratt32 program. Berlin: Berlin Neutron Scattering Center (BENSC), Hahn–Meitner Institut; 1997.
[29] Parratt LG. Phys Rev 1954;95:359–69.
[30] Cahn JW, Hilliard JE. J Chem Phys 1958;28:258–67.
[31] Cahn JW. J Chem Phys 1965;42:93–9.
[32] Bhatia Q, Pan D, Koberstein J. Macromolecules 1988;21:2166–75.
[33] Cowie J, Devlin B, McEwen I. Macromolecules 1993;26:5628–32.
[34] Lee S, Sung C. Macromolecules 2001;34:599–604.
[35] Forrey C, Koberstein J, Pan DH. Interface Sci 2003;11:211–23.
[36] Kawaguchi D, Tanaka K, Kajiyama T, Takahara A, Tasaki S. Macromolecules 2003;36:6824–30.
[37] Jones RAL, Norton LJ, Kramer EJ, Bates FS, Wiltzius P. Phys Rev Lett 1991;66:1326–9.
[38] Shull KR, Mayers AM, Russell TP. Macromolecules 1993;26:3929–36.